Nigerian Research Journal of Engineering and Environmental Sciences 9(2) 2024 pp. 825-840
p ISSN: 2635-3342; e ISSN: 2635-3350

Nigerian Research Journal of Engineering and Environmental Sciences
Journal homepage: www.rjees.com

Original Research Article

Beneficiation and Characterization of High-Purity Nano Calcite from a Carbonaceous Mineral

***[1]Onovo, H.O., [1]Mgbemere, H.E., [1]Agbeleye, A.A., [2]Akano, T.T. and [1]Iheme, C.O.**

[1]Department of Metallurgical and Materials Engineering, Faculty of Engineering, University of Lagos, Akoka, Lagos, Nigeria.
[2]Deparment of Mechanical Engineering, University of Botswana, Gaborone, UB 0022, Botswana.
*honovo@unilag.edu.ng

http://doi.org/10.5281/zenodo.14566264

ARTICLE INFORMATION

Article history:
Received 14 Oct. 2024
Revised 06 Dec. 2024
Accepted 07 Dec. 2024
Available online 30 Dec. 2024

Keywords:
Beneficiation
Froth flotation
Carbonate mineral
Higher-grade nano calcite
Sedimentary environments
Swelling property

ABSTRACT

This study investigated the beneficiation of calcite ore to obtain a high-purity nano calcite suitable for industrial applications using the froth flotation process. The physicochemical properties of untreated and treated calcite were analyzed and compared with Nigeria Industrial Standards (NIS). X-ray fluorescence (XRF) analysis was employed to assess the elemental composition of the purified calcite across varying pH levels. The results showed significant improvements in treated calcite, including increased purity (72.5%) and higher calcium oxide content (25.5%), surpassing NIS requirements. These improvements were attributed to the effectiveness of the froth flotation process in removing impurities, yielding a higher-grade product. The treated nano calcite displayed a pH value of 8.4, meeting the NIS range of 7.5–10.5, and a density within the standard range of 1.5–1.6 g/cm³. The XRF analysis revealed pH-dependent trends, such as increased elemental concentrations at lower pH levels, while variations in scavenger and cleaner concentrations showed no distinct patterns. Additionally, particle size analysis revealed a bimodal distribution, with two dominant size distributions: smaller nanoparticles (~1–10 nm) and larger particles (~100 nm), with the latter dominating the volume distribution. X-ray diffraction (XRD) analysis confirmed calcite as the primary mineral phase, evidenced by sharp, well-defined peaks indicative of excellent crystallinity. Minor phases such as quartz, lime, and muscovite were also identified. This study emphasizes the potential of local calcite deposits to reduce import dependency, lower production costs, and drive economic growth.

1. INTRODUCTION

Calcite ($CaCO_3$), a widely distributed carbonate mineral, is one of nature's most abundant and versatile minerals. Forming part of the Earth's sedimentary, metamorphic, and igneous geological frameworks,

calcite contributes significantly to the composition of rocks such as limestone and marble (Chen *et al.*, 2013; Huang et al., 2022). Its importance is highlighted by its role as a primary reservoir in the planet's crust, influencing geological, ecological, and industrial systems. Calcite's unique properties and global distribution have made it a key subject of research and industrial use (Xu *et al.*, 2022; Wang *et al.*, 2024). Calcite exhibits a trigonal crystal structure formed by $[CO_3]^{2-}$ coordination triangles, where carbonate groups interact with calcium ions. When subjected to mechanical stress, this structure imparts distinctive properties, such as birefringence, fluorescence under UV light, and triboluminescence (Kaya *et al.*, 2023). Calcite typically occurs as colorless or white crystals in its pure form. However, trace elements, such as magnesium, iron, and manganese, can impart colors ranging from pink to green, further enhancing its aesthetic and economic value (Hayakawa *et al.*, 2008).

In sedimentary environments, calcite is often associated with dolomite, gypsum, quartz, and anhydrite. In hydrothermal veins, it is found alongside minerals like pyrite, fluorite, and chalcopyrite (Wonyen *et al.*, 2018). Such associations necessitate beneficiation techniques to separate calcite from other minerals, ensuring its suitability for high-value applications (Faramarzpour *et al.*, 2022; Huang et al., 2022). Calcite is a key material in numerous industries due to its versatile properties. In the paper industry, it is used as a filler and coating material, improving opacity, brightness, and printability (Emergen Research, 2020). In plastics, calcite enhances strength and reduces production costs, while in paints and coatings, it improves durability and finish quality. Additionally, calcite is essential in agriculture, where it neutralizes acidic soils and promotes crop health (Cosentino *et al.*, 2020; Fu *et al.*, 2022).

Beyond traditional uses, nanosized calcite has emerged as a high-performance material in modern industries. Its ultra-fine particle size increases its surface area and reactivity, enabling its use in advanced composites, coatings, and environmental remediation (Cao *et al.,* 2019; Sharma and Ashish 2023). The global calcite market was valued at USD 10.19 billion in 2019 and is projected to grow to USD 14.99 billion by 2027, driven by increasing demand in the construction and agricultural sectors (Emergen Research, 2020).

Nigeria has significant calcite deposits across various states, including Ogun, Cross River, Benue, Ebonyi, and Enugu. These resources remain largely untapped, with minimal industrial exploitation. In 2016, Nigeria imported over 51,000 tonnes of calcite and related minerals to meet domestic demand. This reliance on imports presents a significant economic challenge, particularly when domestic calcite deposits could be utilized for local industrial applications. Calcite in Nigeria often occurs with impurities, necessitating beneficiation techniques like froth flotation to achieve the high purity required for industrial uses (Shariati *et al.*, 2015; Teawpanich *et al.*, 2023). Furthermore, nanosized calcite production remains limited due to the lack of advanced processing technologies (Ali *et al.*, 2022). Addressing these challenges could position Nigeria as a key player in the global calcite market, reducing production costs and fostering economic growth.

Calcite's beneficiation and characterization are critical for unlocking its full industrial potential. Beneficiation processes like froth flotation help separate calcite from associated minerals and impurities, ensuring high purity and uniform particle size. Characterization techniques such as Scanning Electron Microscopy (SEM), Energy Dispersive X-ray (EDX), and X-ray Fluorescence (XRF) provide insights into calcite's morphological and chemical properties, facilitating its use in specialized applications (Ali *et al.*, 2011 and Huang *et al.*, 2021).

High-purity nanosized calcite is particularly valuable in advanced materials. Its enhanced surface area and reactivity make it ideal for improving the performance of cement, polymers, and coatings (Garg *et al.*, 2021; Chuzeville *et al.*, 2022). By leveraging local calcite resources, Nigeria can reduce its reliance on imports, foster sustainable industrial growth, and create new economic opportunities (Masindi *et al.*, 2022; Mishra *et al.*, 2022). The objectives of this study are to exploit Nigerian calcite deposits for industrial applications, to purify calcite from associated minerals through froth flotation, to characterize the morphological and chemical properties of calcite using SEM and XRF, and to evaluate the suitability of processed calcite for cement production and other industrial applications. This study addresses

critical gaps in Nigeria's calcite beneficiation processes, aligning with global trends in advanced material development. The research contributes to technological innovation by focusing on nanosized calcite while promoting sustainable resource utilization. The outcomes are expected to enhance the competitiveness of Nigerian industries and support the country's economic diversification efforts.

2. MATERIALS AND METHODS

2.1. Materials

The study employed lime, corn starch, pine oil, distilled water, and hydrochloric acid as reagents. Raw calcite (calcium carbonate) served as the primary material. The processing equipment consisted of a jaw crusher, a laboratory jaw crusher, a ball mill, sieves, a sieve shaker, and a flotation cell.

2.2. Raw Material Collection and Pulverization

Raw carbonate mineral (Calcite - $CaCO^3$) (Figure 1a) was purchased from Akure, Ondo State, Nigeria. A preliminary test was conducted by reacting a few ore grains with 10% hydrochloric acid. The presence of effervescence confirmed the presence of calcium carbonate. The process of crushing calcite was carried out using a jaw crusher, which employs a stationary jaw plate and a moving jaw plate to break the material into smaller fragments. The raw calcite was prepared as large chunks or blocks for crushing. The jaw crusher was securely positioned on a stable base. The stationary jaw plate was fixed vertically, while the moving one was aligned to exert pressure during the operation. The crusher's feed opening was adjusted to determine the maximum size of calcite chunks that could be processed.

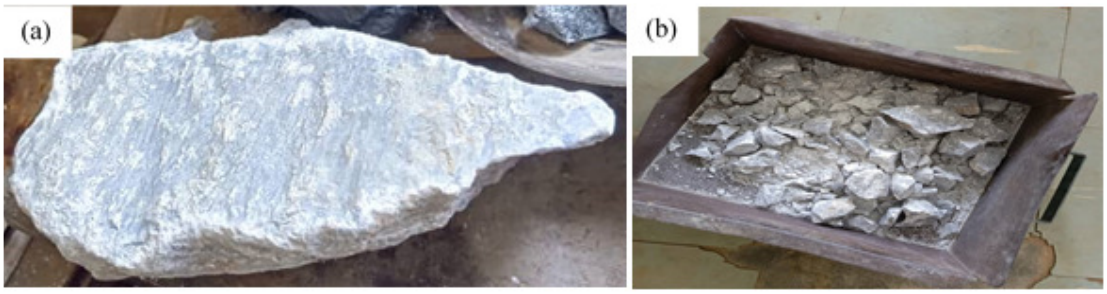

Figure 1: Calcite ore (a) as received, and (b) after first stage crushing

Calcite chunks were fed into the crusher through the feed opening. The moving jaw plate applied pressure against the stationary plate, crushing the calcite into smaller particles. The calcite underwent repeated crushing cycles, with each cycle further reducing particle size. The crushed calcite particles, now reduced in size (Figure 1b), were discharged from the bottom of the crusher. The particles were collected in a container for subsequent milling processing. The milling process for calcite involves using a rotating cylindrical chamber filled with spherical grinding media (balls) to reduce the size of calcite particles. After the crushing process, calcite exists as large chunks, blocks, or powder, depending on the initial particle size and desired final size. The machine consists of a rotating cylindrical chamber, made of steel, driven by a motor, and a suitable drive system. Grinding media (balls) were introduced into the chamber. These media are harder than calcite to ensure effective milling. The size, material, and composition of the grinding media were selected based on the desired outcome. The calcite sample is evenly distributed among the grinding media within the chamber. The sample occupied only a fraction of the chamber's total volume, leaving sufficient space for effective milling action. The ball milling machine is activated, causing the chamber to rotate. As the chamber rotates, the grinding media cascades and tumbles, exerting impact and compressive forces on the calcite particles. This repeated action results in the comminution of calcite particles, progressively reducing their size and achieving a specific particle size distribution. The ball milling machine was stopped once the desired milling duration was reached. The calcite samples were carefully removed from the chamber and separated from the grinding

media. The sample is cleaned and inspected through a sieving process to confirm that the required particle size reduction has been achieved.

2.3. Sieving Process

After the ball milling process, a sieving step was employed to separate the milled calcite particles into fractions of different sizes using a sieve shaker machine. A set of sieves with three different mesh 120, 60, and 40 mesh (125, 250, and 400 microns) sizes were prepared. The mesh size determines the openings in each sieve, allowing particles smaller than the mesh size to pass through. The sieves were stacked in descending order of mesh size, with the largest mesh size on top and the smallest at the bottom. A collection pan was placed beneath the bottom sieve to collect any remaining fine particles. The milled calcite sample was carefully placed into the top sieve, ensuring an even distribution across its surface. The sieve shaker machine was activated, initiating a vibrating or oscillating motion. The vibration caused the calcite particles to move and pass through the sieves based on their size. Particles smaller than each sieve's openings passed to the next layer, while larger particles remained on top. After the sieving process was complete, each sieve was carefully removed from the stack, and the calcite particles collected on each sieve were transferred to separate collection pans corresponding to their size fraction.

2.4. Froth Floatation Process

The froth flotation process is widely used to separate valuable minerals from their ores. It relies on the differences in surface properties of minerals to selectively separate them using the principle of hydrophobicity. The ground ore was mixed with water in a conditioning tank, and reagents are added to modify the surface properties of the minerals. These reagents include collectors (pine oil), depressants (corn starch), pH modifiers (such as sulfuric acid), and other modifiers (such as lime). The conditioned ore slurry was introduced into a flotation cell, which was then agitated to promote the interaction between air bubbles and mineral particles. Compressed air is introduced into the cell, generating bubbles that attach to the hydrophobic mineral particles. The resulting froth, containing a high concentration of valuable minerals, was continuously or intermittently removed from the cell and collected in a launder. The remaining slurry, known as tailings, contains hydrophilic minerals and other impurities. Proper tailings disposal is essential to minimize environmental impact and comply with regulations.

2.5. Drying Process

After the froth flotation process, the concentrate obtained needs to be dried to remove excess water and prepare it for further processing or storage. The froth, containing valuable minerals, was collected from the flotation cell and transferred to a storage container or a thickener for further processing. The first step in the drying process typically involves filtration or dewatering to remove excess water. Once dewatered, the concentrate is further dried using the sun (Figure 3a) and thermal methods (Figure 3b). Heat evaporates the remaining moisture, carried away by air or gas flow. Once the drying process is completed, the concentrate is dried, which produces a stable nano calcite product suitable for storage, transportation, or further processing, depending on the specific application and requirements.

Figure 2: Froth floatation collection process

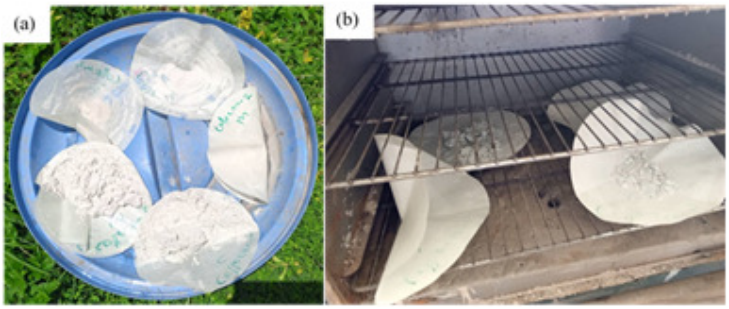

Figure 3: Purified calcite drying processes

2.6. Determination of Calcite pH and Conductivity

The pH of the calcite was measured using a multimeter electrode at 28 °C. The multimeter was used to determine pH, conductivity, and total dissolved solids (TDS) by switching to the appropriate settings, as shown in Figure 4. The pH reading obtained was 6.8.

2.7. Determination of Moisture Content

Some quantity (1 g) of the sample was weighed into a clean beaker (W_1) and placed in an oven at 105°C for about 2 hours until a constant weight was achieved. The beaker was then transferred to a desiccator to cool and reweighed (W_2). The difference in weight represents the amount of water lost from the sample. Equation 1 was used to estimate the percentage moisture content of the calcite.

Figure 4: pH test using multimeter

$$\%\ \text{Moisture content} = \frac{W_1 - W_2}{mass\ of\ sample} * 100 \quad (1)$$

Where W_1 and W_2 are the respective weights of the sample and beaker before drying and after oven drying.

2.8. Determination of Bulk Density

Some sample (5 g) was weighed and placed into a measuring cylinder. The open end of the cylinder was sealed with cellophane paper, and the cylinder was tapped continuously on a solid base until the sample was packed with no air gaps. The cylinder was then weighed, and the volume of the packed sample was recorded. The density of the sample was calculated using the Equation 2.

$$\text{Density } (\text{g/cm}^3) = \frac{W_2 - W_1}{volume\ of\ sample} * 100 \quad (2)$$

Where W_1 and W_2 are the weight of the empty measuring cylinder and the weight of the measuring cylinder with the packed sample.

2.9. Determination of Percentage Purity

Some powder sample (2 g) was placed into a 250 ml conical flask. Then, 10 ml of 2 M HCl was added, releasing CO_2 as effervescence. Afterward, 25 ml of deionized water was added, and the solution was heated in a water bath to a temperature of 70 °C. The solution was then allowed to cool before being titrated with 0.1 M of ethylenediaminetetraacetic acid (EDTA) and buffered with ammonium hydroxide, using murexide as an indicator. A violet colour change indicated the endpoint of the titration. The percentage purity of the sample was measured using Equation 3.

$$\%\ Purity = \frac{Titre\ value * (0.1M\ EDTA)}{Mass\ of\ sample} * 100 \quad (3)$$

2.10. Analysis of Chemical Composition using XRF

The chemical composition of the calcite samples was analyzed using X-ray fluorescence (XRF). Each sample was crushed using an electric crusher and pulverized for 60 seconds with a Herzog Gyro-mill (Simatic C7-621). Pellets were prepared by grinding 20 g of the pulverized sample with 0.4 g of stearic acid for 60 seconds. After each grinding session, the gyro mill was thoroughly cleaned to prevent contamination. For pellet preparation, 1 g of stearic acid was weighed into an aluminum cup to serve as a binding agent. The aluminum cup was then filled with the sample to the marked level. The cup was transferred to a Herzog pelletizing machine and subjected to a pressure of 200 kN for 60 seconds. The resulting 2 mm pellets were placed into the sample holder of the XRF equipment (Philips PW-1800) for analysis.

2.11. Scanning Electron Microscope (SEM)

The Phenom ProX SEM-EDS microscope was powered on and allowed to warm up for 15 minutes. An aluminum holder stub was cleaned with ethanol and dried using compressed air. A small piece of sticky carbon tape was applied to the center of the stub. A small portion of the processed calcite sample was then placed on the carbon tape, and the sample surface was coated with a thin layer of gold using a sputter coater to ensure conductivity. The sample was labeled and dried in an oven at 60 °C for 10 minutes. The nitrogen line to the SEM was opened, and the vent button was pressed to purge the chamber with nitrogen gas. The sample holder stub was placed in the SEM sample chamber, and the door was closed. The rotary pump was activated, creating a vacuum of 5×10^{-5} Pa in the chamber. Once the vacuum was achieved, the filament light was turned on, and the monitor automatically powered up. The accelerator voltage was set to 15 kV, but the filament burned out during operation. The sample was scanned at an initial magnification 10x to observe the overall surface morphology. The magnification was then increased incrementally to 500x, 1000x, and 1500x to capture detailed surface images. This analysis was performed on calcite samples with varying pH values (4.5, 5.5, and 6.5).

2.12. Determination of Specific Gravity by Pycnometer Method

The Le Chatelier flask method is used technique for determining the specific gravity of solid materials. Specific Gravity (S.G.) measures a material's density relative to water. A specific gravity of 1.0 indicates that the material has the same density as water; a specific gravity greater than 1.0 means the material is denser than water and will sink, whereas a specific gravity less than 1.0 means the material is less dense than water and will float. The Le Chatelier flask (or pycnometer) was cleaned and dried thoroughly to ensure it contained no traces of liquid or moisture. The dry, empty flask with its stopper was weighed, and the weight was recorded as W_1. Approximately 10 g of the sample was added to the flask, filling it to about half its capacity. The flask was stoppered, and its weight was recorded as W_2. Kerosene was added to the flask until it was filled to the marked level. The mixture was thoroughly mixed to eliminate air bubbles, and the flask was stoppered and weighed, recorded as W_3. The flask was emptied, cleaned, and refilled to the marked level with kerosene. The flask was then weighed, and the weight was recorded as W_4. Equation 5 was used to deduce the calcite's specific gravity (S.G.).

$$S.G = \frac{W_2 - W_1}{(W_2 - W_1) - (W_3 - W_4)} * 0.79 \quad (4)$$

where 0.79 is the specific gravity of kerosene.

3. RESULTS AND DISCUSSION

The physicochemical properties of the analyzed calcite are summarized in Table 1. The treatment process significantly increased calcite purity from 62.5% to 72.5%. Using reagents to separate impurities like pyrite and quartz, the flotation process is crucial for achieving high-purity calcite. The treated calcite has a higher calcium oxide content (25.5%) than the raw calcite (15.2%), making it more suitable for cement and paint industries. While the treated calcite meets the minimum standard of 22% calcium oxide, the raw calcite falls short. The treatment process enhances the quality of calcite, making it more suitable for various industrial applications, particularly cement production.

Table 1: Properties of untreated and treated calcite

SN	Parameter	Nis Standard	Raw Calcite	Treated Calcite
1	Appearance	Pure white fine powder	Off-white coarse powder	White fine powder
2	pH	7.5 – 10.5	6.8	8.4
3.	Test with 10% HCl	Effervescence	Conform	Conform
4.	Conductivity (mS/cm)	NS	0.12	0.08
5.	Density (g/cm^3)	1.5 – 1.6	1.77	1.51
6.	Swelling Property	NS	13.8	12.4
7.	Moisture (%)	5 % max	4	3
8.	Purity (%)	70 % min	62.5	72.5
9.	Calcium oxide (%)	22 % min	15.3	25.5

The results presented in Figure 5 reveal intriguing trends in the yield of purified calcite across different pH levels. The yield of the Weight Rougher fraction exhibited a slight decrease as the pH decreased, suggesting that lower pH levels may influence the abundance of components within this fraction. This observation is consistent with studies highlighting the role of acidic environments in modifying mineral surface properties and elemental distribution (Lerman and Mackenzie, 2018). In contrast, the Scavenger concentration displayed variability across the pH range without a clear trend, indicating the need for further analysis to identify potential correlations. Similarly, the Cleaner concentration also showed variability without a distinct pattern, aligning with reports of complex, pH-dependent behaviors in mineral processing systems (Ashraf *et al*., 2018).

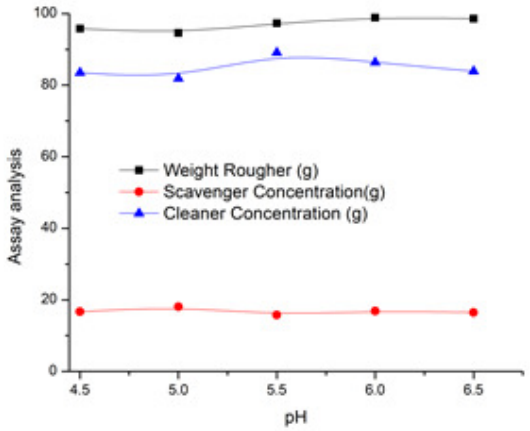

Figure 5: Calcite yield at varied pH levels and constant feed: weight (200 g) and assay (49 g) particulates at various pH levels

Figure 6 illustrates that increasing the collector dosage generally results in a decrease in the concentrations of Weight Rougher, Scavenger, and Cleaner fractions. This trend suggests that higher collector dosages may enhance the separation efficiency of specific components, thereby reducing their presence in purified calcite. These observations align with previous findings that demonstrate the impact of collector dosage on the selectivity and efficiency of froth flotation processes (Ba-Abbad *et al.*, 2013). The yield analysis further examines calcite yields at varying pH levels. At pH 4.5 and 5.0, XRF intensity increases with decreasing pH, signifying higher yields under more acidic conditions. This supports findings that acidic environments often promote the release of specific ions from mineral surfaces (Balaram and Sawant, 2022). At pH 5.5, the yield remains relatively low, except for a sudden increase at around 1050 eV, which may indicate the presence of a specific element. Similarly, at pH 6.0, a noticeable increase in yield is observed. In contrast, at pH 6.5, the yield remains low, with a sharp increase near 2300 eV, again suggesting the presence of specific elements. These results underscore the influence of pH on calcite purification, with lower pH levels (acidic conditions) generally yielding higher outputs, while higher pH levels (alkaline conditions) correspond to reduced yields. These findings highlight the importance of pH as a critical factor in controlling elemental composition and optimizing calcite purification processes.

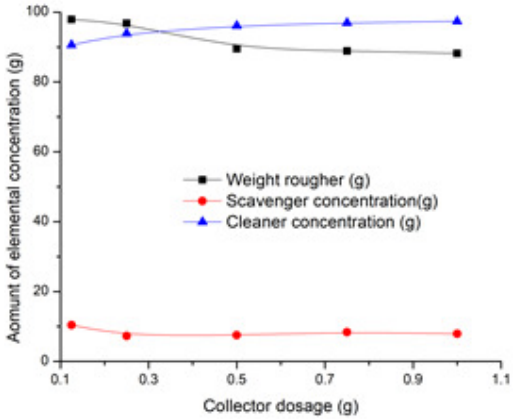

Figure 6: Collector dosage analysis for beneficiation of nano calcite particulates at constant feed: weight (200) and assay (49)

The weight rougher froth flotation process represents the initial stage in froth flotation, primarily aimed at separating and concentrating the bulk of the valuable mineral from calcite ore. This stage produces a preliminary concentrate, known as the rougher concentrate, which serves as a basis for further

refinement (Crispen et al., 2022). Following this, the Scavenger Concentration refers to the recovery of additional valuable mineral particles during the scavenger stage of froth flotation. This stage captures particles missed in the rougher stage, typically resulting in a lower-grade concentrate that requires further processing to meet desired quality standards (Radmehr et al., 2018). Lastly, the Cleaner Concentration is the final, purified product from froth flotation. It is achieved by further processing the rougher concentrate in dedicated cleaning stages, where impurities are removed to obtain a high-grade mineral product. This step ensures the enrichment of the desired mineral while minimizing residual gangue content (Whitworth et al., 2022; Jera and Bhondayi, 2022).

The results in Figure 7 revealed interesting trends in the elemental composition of purified nanocalcite. The most prominent element in Figure 7 is Calcium (Ca), with a concentration exceeding 80%. This is expected as nanocalcite is a calcium carbonate nanomaterial, and calcium is a major constituent of calcium carbonate. Other elements present in minor concentrations include: Mg ~ 15%, Al ~ 2%, Si ~ 1%, P ~ 0.5%, S ~ 0.5%, Fe ~ 0.5%, Ni ~ 0.5%, Cu ~ 0.5%, Zn ~ 0.5%, Mo ~ 0.5%, Sn ~ 0.5%, and Sb ~ 0.5%. The presence of minor elements likely results from impurities or additives during the synthesis process.

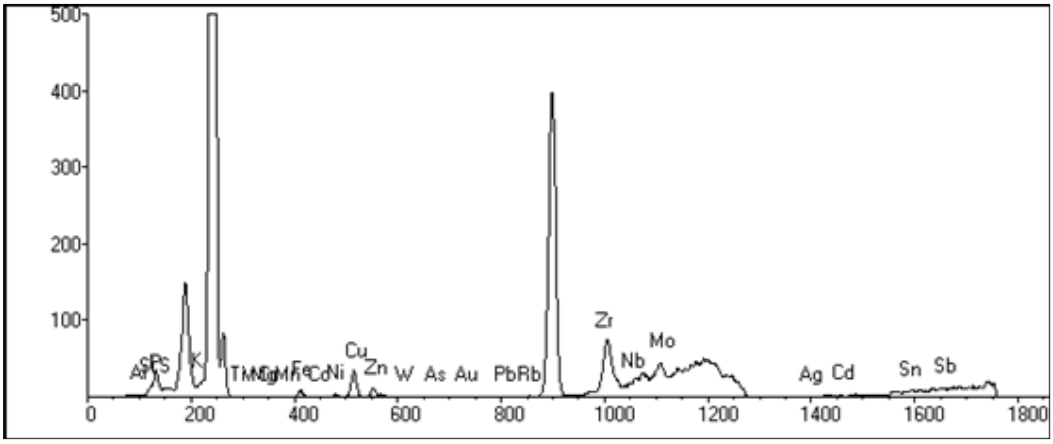

Figure 7: XRF spectra of nanocalcite particulates

The SEM micrograph in Figure 8(a-c) presents a cluster of particles with varying morphologies and sizes. The particles appear to be irregularly shaped, with some exhibiting angular features. The overall texture suggests a heterogeneous mixture, likely due to the dynamic nature of the froth flotation process.

Figure 9 shows a positive linear correlation between the specific gravity of nano calcite particles and the pH level. As the pH increases, the specific gravity generally increases as well. The linear fit line suggests a consistent trend in the data, indicating that the relationship between pH and specific gravity is likely linear within this range. The data points are relatively close to the linear fit line, suggesting a good fit and a strong correlation. Similar trends have been observed in other studies investigating pH-dependent density changes in nanomaterials, where chemical and structural modifications impact specific gravity (Yang *et al.*, 2021). The increase in specific gravity with increasing pH could be due to several factors, such as ion exchange. At higher pH levels, increased ion exchange between the nano calcite particles and the surrounding solution could incorporate heavier ions into the crystal lattice, thereby increasing overall density. This phenomenon has been reported in carbonate systems, where ion substitution is influenced by pH (Ostadrahimi *et al.*, 2021). Another consideration could be particle aggregation. Higher pH might promote the aggregation of nano calcite particles, resulting in larger particles with higher specific gravity. Particle aggregation mechanisms under varying pH conditions have been highlighted in recent research, emphasizing their role in altering material properties (Jiang, 2023; Foroutan *et al.*, 2021). Additionally, changes in crystal structure may also play a role. pH fluctuations could influence the nano calcite's crystal structure, potentially leading to denser crystal

packing at higher pH values. Structural modifications in carbonate minerals caused by pH changes have been documented, further supporting this explanation (Molnár *et al.*, 2023).

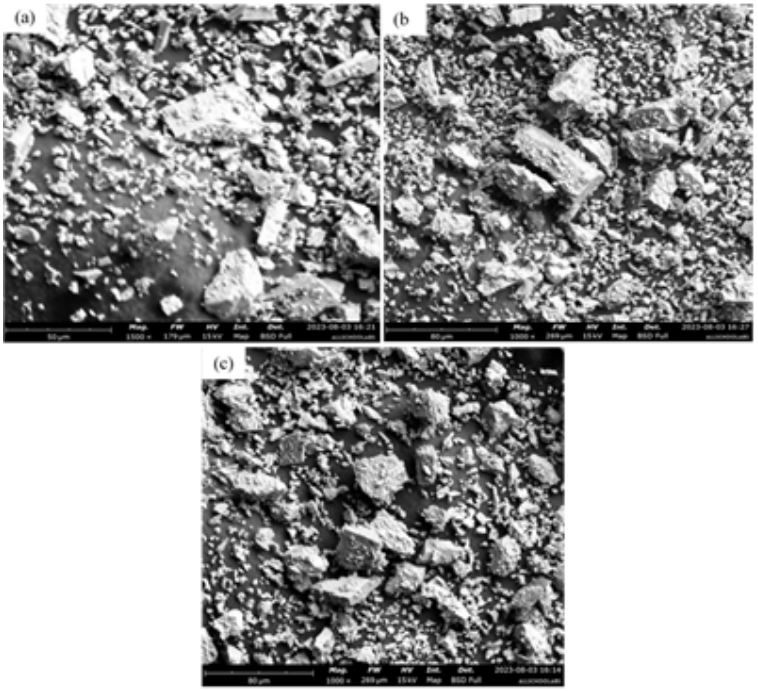

Figure 8: SEM micrograph for nanosized calcite with pH (a) 4.5, (b) 5.5 and (c) 6.5

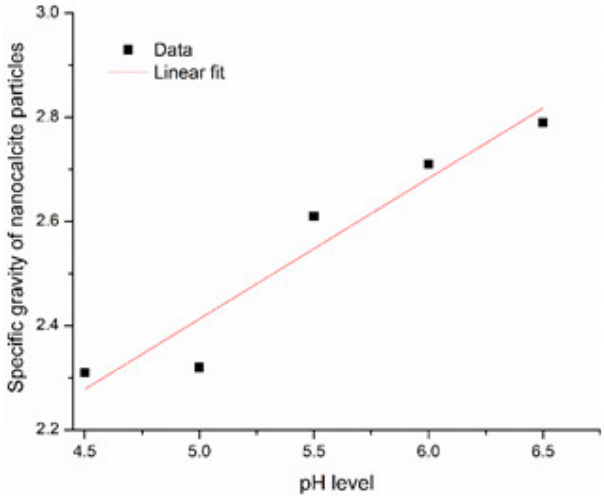

Figure 9: Specific gravity of nano calcite particulates at different pH

Figure 10 (a-c) displays a bimodal distribution, indicating the presence of two distinct peaks in the particle size distribution. This suggests two main populations of particles with different sizes. The first peak is centered around 1–10 nm, representing a significant population of smaller nanoparticles, while the second peak is centered around 100 nm, corresponding to a population of larger particles. The volume distribution is skewed towards the larger particles, as evidenced by the higher peak around 100 nm. This indicates that these larger particles occupy a larger portion of the total volume of the sample. The particle size range extends from approximately 1 nm to 10,000 nm, encompassing very small nanoparticles and larger microparticles. Such broad distributions are common in multi-modal systems

and have been attributed to complex particle formation processes (Letzel *et al*., 2018). The observed bimodal distribution may result from dual nucleation and growth mechanisms, leading to two distinct particle populations. Additionally, smaller nanoparticles may aggregate into larger particles, contributing to the peak at around 100 nm. Aggregation phenomena in nanomaterials have been shown to play a critical role in altering size distributions, as highlighted by Shen *et al*., 2019. The specific experimental conditions, including temperature, stirring rate, and reagent concentration, likely influence this distribution. For instance, parameter variations can significantly impact nucleation rates and particle growth dynamics (Doi *et al*., 2019). Figure 8 provides valuable insights into the particle size distribution of nano calcite at pH 4.5. However, further investigation is necessary to elucidate the underlying mechanisms responsible for the observed bimodal distribution.

Similarly, Figure 11 (a-c) analyzes the calcite samples' X-ray diffraction (XRD) pattern at pH 4.5, 5.5, and 6.5, respectively. The most prominent peaks in the pattern correspond to calcite, the main mineral phase in the sample. These sharp and well-defined peaks indicate good crystallinity of the calcite phase. This observation aligns with recent findings highlighting the correlation between peak sharpness in XRD patterns and crystallinity in mineral phases (Bunaciu *et al*., 2015). In addition to calcite, several minor phases are present in the sample, as indicated by the weaker peaks. These minor phases include quartz, lime, orthoclase, and muscovite. The positions of the peaks correspond to the characteristic d-spacings of the different mineral phases, consistent with methods used to identify minerals in XRD studies (Guanira *et al*. 2020; Santamaría-López and Suárez 2024).

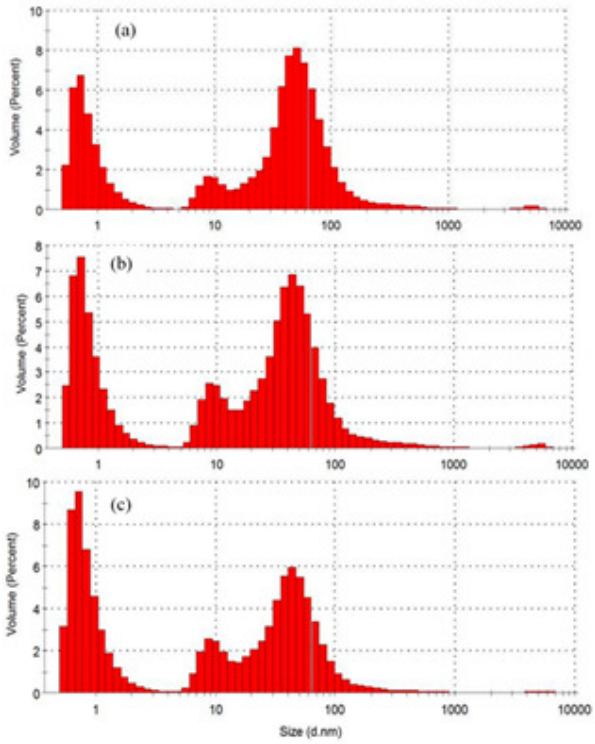

Figure 10: Particle size distribution by volume of calcite at varied pH (a) 4.5, (b) 5.5, and (c) 6.0 level

The relative intensities of the peaks reflect the abundance of each mineral phase in the sample. The strong calcite peaks indicate that it is the dominant phase, while the weaker peaks of the other minerals suggest that they are present in smaller amounts. The presence of minor phases in the calcite sample could be due to several factors: (a) if the starting materials used to synthesize the calcite contained impurities, these impurities might be incorporated into the final product (Forbes *et al*., 2011; Adavi and Dehkordi 2021); (b) if the synthesis process was not carried out under optimal conditions, some of the

starting materials might not have fully transformed into calcite, resulting in the presence of residual phases; and (c) after the synthesis of calcite, secondary reactions might occur, leading to the formation of new mineral phases. The XRD patterns provide valuable information about the mineral composition and crystallinity of the calcite sample at pH 4.5, 5.5, and 6.5. This information can be critical for tailoring calcite for specific industrial applications by identifying and minimizing undesirable phases during synthesis or beneficiation (Gausmann *et al.*, 2020; Ali *et al.*, 2022; Chen et al., 2024).

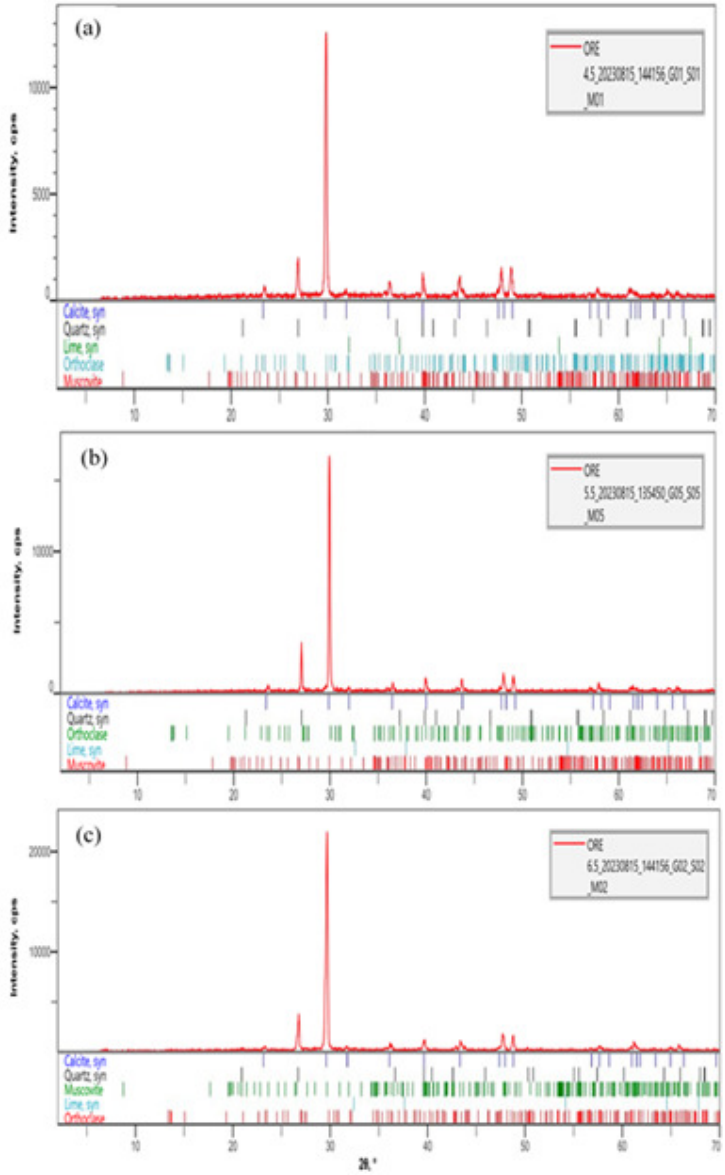

Figure 11: XRD pattern of the calcite at varied pH (a) 4.5, (b) 5.5, and (c) 6.5 level

Figure 12 shows the presence of minor phases such as quartz, lime, orthoclase, and muscovite. However, Figure 11 juxtaposes all the phases observed, which appear in varying proportions across different pH levels. Quartz and orthoclase show a slight increasing trend with increasing pH, while lime and muscovite remain relatively stable. These trends align with studies that emphasize how mineral stability and solubility vary with pH, influencing their distribution in multi-mineral systems (Katsenovich *et al.*, 2021; Sabur *et al.*, 2022). The most striking observation is the dominance of calcite

across all pH levels. The calcite content consistently remains above 70%, indicating that calcite is the primary mineral phase in the samples. While nano calcite remains dominant, there are slight variations in its content with changing pH values. Specifically, there is a general decreasing trend in calcite content from pH 4.5 to pH 6.5. Such variations are likely influenced by the differential solubility of minerals at varying pH levels. As the pH increases, some minerals may dissolve, resulting in a decrease in their content and a relative increase in others, as supported by the findings of Kaszuba *et al.*, (2013). Moreover, chemical reactions between minerals and the solution might occur at different pH levels, leading to the formation or dissolution of certain phases. This is consistent with studies demonstrating that solution chemistry plays a critical role in the precipitation and dissolution of mineral phases during pH-dependent reactions (Holgersson *et al.*, 2024). These findings provide valuable insights into the interplay between pH, solubility, and mineral phase distribution in complex systems like nano calcite samples.

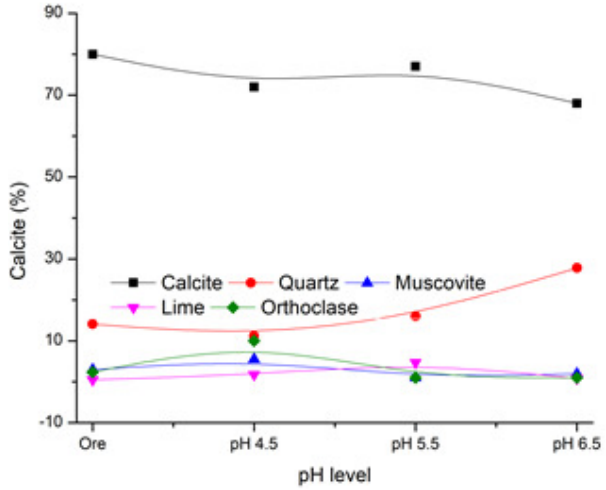

Figure 12: Phases present in nano calcite particulates at different pH level

4. CONCLUSION

Using the froth flotation process, the beneficiation of calcite ore demonstrated significant potential for producing high-quality calcite suitable for industrial applications. Comparative analysis of the physiochemical properties revealed substantial improvements in the purified calcite. The treated calcite achieved a remarkable purity level of 72.5%, surpassing the 62.5% purity of raw calcite, and exhibited a calcium oxide content of 25.5%, exceeding the Nigeria Industrial Standards (NIS) minimum requirement of 22%. These enhancements underscore the effectiveness of the flotation process in selectively removing impurities and upgrading the calcite to meet industrial specifications. XRF analysis further elucidated the elemental composition of the purified calcite across various pH levels. While no consistent trends were observed in the scavenger and cleaner concentrations, a slight decline in rougher concentrations was noted with decreasing pH. This highlights the need for further research to identify and optimize the interplay between pH variations and reagent concentrations to maximize process efficiency. The findings establish a strong foundation for the beneficiation of calcite ore and open avenues for additional studies to refine and scale the process for broader industrial adoption.

5. ACKNOWLEDGMENT

The authors would like to thank the laboratory staff of the Department of Metallurgical and Materials Engineering, Federal University of Technology, Akure, for their invaluable assistance and for providing access to essential equipment, including the Froth Flotation Cell Machine and Sieve Shaker. Additionally, we extend our appreciation to the Department of Metallurgical and Materials Engineering,

University of Lagos, for their foundational support, which significantly contributed to the success of this work.

6. CONFLICT OF INTEREST

There is no conflict of interest associated with this work.

REFERENCES

Adavi, K. and Dehkordi, A. M. (2021). Synthesis and polymorph controlling of calcite and aragonite calcium carbonate nanoparticles in a confined impinging-jets reactor. *Chemical Engineering and Processing - Process Intensification.* 159, 108239, https://doi.org/10.1016/j.cep.2020.108239.

Ali, A., Chiang, Y. W. and Santos, R. M. (2022). X-ray Diffraction Techniques for Mineral Characterization: A Review for Engineers of the Fundamentals, Applications, and Research Directions. *Minerals*, *12*(2), 205. https://doi.org/10.3390/min12020205

Ali, M., Ahmed, S. and Akhtar, N. (2022). Advanced techniques in calcite beneficiation for industrial applications. *Minerals Engineering, 181*, 107520. https://doi.org/10.1016/j.mineng.2022.107520.

Ashraf, M. A., Peng, W., Zare, Y. and Rhee, K. Y. (2018). Effects of Size and Aggregation/Agglomeration of Nanoparticles on the Interfacial/Interphase Properties and Tensile Strength of Polymer Nanocomposites. *Nanoscale Research Letters*, 13, 214. https://doi.org/10.1186/s11671-018-2624-0

Ba-Abbad, M. M., Kadhum, A. H., Mohamad, A. B., Takriff, M. S. and Sopian, K. (2013). The effect of process parameters on the size of ZnO nanoparticles synthesized via the sol–gel technique, *Journal of Alloys and Compounds*, 550, pp. 63-70. https://doi.org/10.1016/j.jallcom.2012.09.076.

Balaram, V. and Sawant, S. S. (2022). Indicator Minerals, Pathfinder Elements, and Portable Analytical Instruments in Mineral Exploration Studies. *Minerals*, *12*(4), 394. https://doi.org/10.3390/min12040394

Bunaciu, A. A., Udriştioiu, E. G. and Aboul-Enein, H. Y. (2015). X-ray diffraction: instrumentation and applications. *Critical Reviews in Analytical Chemistry*, *45*(4), pp. 289-99. DOI: 10.1080/10408347.2014.949616. PMID: 25831472.

Cao, M., Ming, X., He, K., Li, L. and Shen. S. (2019). Effect of Macro-, Micro- and Nano-Calcium Carbonate on Properties of Cementitious Composites-A Review. *Materials (Basel)*, *12*(5), 781. doi: 10.3390/ma12050781. PMID: 30866439; PMCID: PMC6427187.

Chen, W. and Simonetti, A. (2013). In-situ determination of major and trace elements in calcite and apatite, and U–Pb ages of apatite from the Oka carbonatite complex: Insights into a complex crystallization history, *Chemical Geology*, 353. pp. 151-172. https://doi.org/10.1016/j.chemgeo.2012.04.022.

Chen, Y., Huang, N., Li, Y., Lu, Y., Jiang, Y., Zhou, Z. and Wang, D. (2024). Physical and chemical processes driven by natural iron minerals in aquatic environments, *Water Cycle*. https://doi.org/10.1016/j.watcyc.2024.10.002.

Chuzeville, L., Boury, F., Duday, D., Anand, R., Moretto, E. and Thomann, J.-S. (2022). Eco-friendly processes for the synthesis of amorphous calcium carbonate nanoparticles in ethanol and their stabilisation in aqueous media. *Green Chemistry*, 24, pp. 1270-1284. https://doi.org/10.1039/D1GC03396D

Cosentino. I., Liendo, F., Arduino, M., Restuccia, L., Bensaid, S., Deorsola, F. and Ferro, G. A. (2020). Nano $CaCO_3$ particles in cement mortars towards developing a circular economy in the cement industry. *Procedia Structural Integrity*, 26, pp. 155-165. https://doi.org/10.1016/j.prostr.2020.06.019.

Crispen, M. T., Willie, N. and Sheunopa, G. (2022). Advances of Nanotechnology Applications in Mineral Froth Flotation Technology. (Eds): Fosso-Kankeu, E., Mkandawire, M. and Mamba B. https://doi.org/10.1002/9781119865360.ch8

Doi, A., Ejtemaei, M. and Nguyen, A. V. (2019). Effects of ion specificity on the surface electrical properties of kaolinite and montmorillonite. *Minerals Engineering*, 143, 105929. https://doi.org/10.1016/j.mineng.2019.105929.

Emergen Research. (2020). Global calcite market to reach USD 14.99 billion by 2027. *Emergen Research*. Retrieved from https://www.emergenresearch.com/press-release/global-calcite-market.

Faramarzpour, A., Samadzadeh Yazdi, M.R., Mohammadi, B. and Chehreh Chelgani, S. (2022). Calcite in froth flotation - A review, *Journal of Materials Research and Technology,* 19, pp. 1231-1241. https://doi.org/10.1016/j.jmrt.2022.05.106.

Forbes, T. Z., Radha, A. V. and Navrotsky, A. (2011). The energetics of nanophase calcite. *Geochimica et Cosmochimica Acta. 75*(24), pp. 7893-7905. https://doi.org/10.1016/j.gca.2011.09.034.

Foroutan, A., Abbas Zadeh Haji Abadi, M., Kianinia, Y. and Ghadiri M. (2021). Critical importance of pH and collector type on the flotation of sphalerite and galena from a low-grade lead–zinc ore. *Scientific Reports*, 11, 3103. https://doi.org/10.1038/s41598-021-82759-3

Fu, Q., Zhang, Z., Zhao, Xu., Xu, W. and Niu, D. (2022). Effect of nano calcium carbonate on hydration characteristics and microstructure of cement-based materials: A review. *Journal of Building Engineering*, 50, 104220. https://doi.org/10.1016/j.jobe.2022.104220.

Garg, R., Kumari, M., Kumar, M., Dhiman, S. and Garg, R. (2021). Green synthesis of calcium carbonate nanoparticles using waste fruit peel extract, *Materials Today: Proceedings*, 46, Part 15, pp. 6665-6668. https://doi.org/10.1016/j.matpr.2021.04.124.

Gausmann, M., Kocks, C., Doeker, M., Eggert, A., Maßmann, T. and Jupke, A. (2020). Recovery of succinic acid by integrated multi-phase electrochemical pH-shift extraction and crystallization, *Separation and Purification Technology*, 240, 116489. https://doi.org/10.1016/j.seppur.2019.116489.

Guanira, K., Valente, T. M., Ríos, C. A., Castellanos O. M., Salazar, L., Lattanzi, D. and Jaime, P. (2020). Methodological approach for mineralogical characterization of tailings from a Cu(Au,Ag) skarn type deposit using QEMSCAN (Quantitative Evaluation of Minerals by Scanning Electron Microscopy), *Journal of Geochemical Exploration.* 209, 106439. https://doi.org/10.1016/j.gexplo.2019.106439.

Hayakawa, S., Hajima, Y., Qiao, S., Namatame, H. and Hirokawa, T. (2008). Characterization of Calcium Carbonate Polymorphs with Ca K Edge X-ray Absorption Fine Structure Spectroscopy. *Analytical Sciences*, *24*(7), pp. 835-837. https://doi.org/10.2116/analsci.24.835.

Holgersson, S., Drake, H., Karlsson, A. and Krall, L. (2024). Biotite dissolution kinetics at pH 4 and 6.5 under anaerobic conditions and the release of dissolved Fe(II), *Chemical Geology*, 662, 122204, ISSN 0009-2541. https://doi.org/10.1016/j.chemgeo.2024.122204.

Huang, J., Zhang, Q., Li, H. and Wang, C. (2022). Difficulties and Recent Achievements in Flotation Separation of Fluorite from Calcite—An Overview. *Minerals*, *12*(8), 957. https://doi.org/10.3390/min12080957

Huang, R. L., S., Zhang, X., Song, Y., He, G., Wang, Z. and Lian, B. (2021). Bio-mineralisation, characterization, and stability of calcium carbonate containing organic matter, *Royal Society of Chemistry Advances*, 11, pp. 14415-14425. DOI: 10.1039/D1RA00615K

Islam, Kh. N., Abu Bakar, Md. Z. B., Noordin, M. M., Hussein, M. Z. B., Abd Rahman, N. S. B. and Ali, Md. E. (2011). Characterisation of calcium carbonate and its polymorphs from cockle shells (Anadara granosa), *Powder Technology*, *213*(1–3), pp. 188-191. https://doi.org/10.1016/j.powtec.2011.07.031.

Jera, T. M. and Bhondayi, C. (2022). A Review on Froth Washing in Flotation. *Minerals*, *12*(11), 1462. https://doi.org/10.3390/min12111462.

Jiang K., Han Y., Liu J., Wang Y., Ge W. and Zhang D. (2023). Experimental and theoretical study of the effect of pH level on the surface properties and floatability of pyrite. *Applied Surface Science*, 615, 156350, https://doi.org/10.1016/j.apsusc.2023.156350.

Kaszuba, J., Yardley, B. and Andreani, M. (2013). Experimental perspectives of mineral dissolution and precipitation due to carbon dioxide-water-rock interactions. *Reviews in Mineralogy and Geochemistry*, *77*(1), pp. 153 - 188. https://doi.org/10.2138/rmg.2013.77.5

Katsenovich, Y. P., Gort, R. T., Gudavalli, R., Szecsody, J., Freedman, V. L. and Qafoku, N. P. (2021). Silicon concentration and pH controls over competitive or simultaneous incorporation of iodate and chromate into calcium carbonate phases, *Applied Geochemistry*, 128, 104941. https://doi.org/10.1016/j.apgeochem.2021.104941.

Kaya, M., Kumral, M., Yalçın, C. and Abdelnasser, A. (2023). Sulfur and Carbon–Oxygen Isotopic Geochemistry and Fluid Inclusion Characteristics of the Yolindi Cu-Fe Skarn Mineralization, Biga Peninsula, NW Turkey: Implications for the Source and Evolution of Hydrothermal Fluids. *Minerals*, *13*(12), 1542. https://doi.org/10.3390/min13121542

Lerman, A. and Mackenzie, F.T. (2018). Carbonate Minerals and the CO_2-Carbonic Acid System. In: White, W.M. (eds) *Encyclopedia of Geochemistry*. *Encyclopedia of Earth Sciences Series*. *Springer, Cham.* https://doi.org/10.1007/978-3-319-39312-4_84

Letzel, A., Gökce, B., Menzel, A., Plech, A. and Barcikowski, S. (2018). Primary particle diameter differentiation and bimodality identification by five analytical methods using gold nanoparticle size distributions synthesized by pulsed laser ablation in liquids. *Applied Surface Science*, 435, pp. 743-751. https://doi.org/10.1016/j.apsusc.2017.11.130.

Masindi, V., Foteinis, S., Renforth, P., Ndiritu, J., Maree, J. P., Tekere, M. and Chatzisymeon, E. (2022). Challenges and avenues for acid mine drainage treatment, beneficiation, and valorisation in circular economy: A review, *Ecological Engineering*, 183, 106740. https://doi.org/10.1016/j.ecoleng.2022.106740.

Mishra, S., Panda, S., Akcil, A., and Dembele, S. (2022). Biotechnological Avenues in Mineral Processing: Fundamentals, Applications and Advances in Bioleaching and Bio-beneficiation. *Mineral Processing and Extractive Metallurgy Review*, *44*(1), pp. 22–51. https://doi.org/10.1080/08827508.2021.1998043.

Molnár, Z., Dódony, I. and Pósfai, M. (2023). Transformation of amorphous calcium carbonate in the presence of magnesium, phosphate, and mineral surfaces, *Geochimica et Cosmochimica Acta*, 345, pp. 90-101. https://doi.org/10.1016/j.gca.2023.01.028.

Ostadrahimi, M., Farrokhpay, S., Gharibi, K. and Dehghani, A. (2021). Effects of Operating Parameters on the Froth and Collection Zone Recovery in Flotation: An Industrial Case Study in a 10 m^3 Cell. *Minerals*, *11*(5), 494. https://doi.org/10.3390/min11050494

Radmehr, V., Shafaei, S. Z., Noaparast, M., & Abdollahi, H. (2018). Optimizing Flotation Circuit Recovery by Effective Stage Arrangements: A Case Study. *Minerals*, *8*(10), 417. https://doi.org/10.3390/min8100417

Sabur, M. A., Parsons, C., T., Maavara, T. and Cappellen, P. V. (2022). Effects of pH and Dissolved Silicate on Phosphate Mineral-Water Partitioning with Goethite, *ACS Earth and Space Chemistry, 6*(1), pp. 34-43. DOI: 10.1021/acsearthspacechem.1c00197.

Santamaría-López, Á. and Suárez, M. (2024). Limits for the Identification of Smectites Mixed with Common Minerals Based on Short-Wave Infrared Spectroscopy. *Minerals*, *14*(11), 1098. https://doi.org/10.3390/min14111098

Shariati, S., Ramadi, A. and Salsani, A. (2015). Beneficiation of Low-Grade Phosphate Deposits by a Combination of Calcination and Shaking Tables: Southwest Iran. *Minerals*, *5*(3), 367-379. https://doi.org/10.3390/min5030367

Sharma, H. and Ashish, D. K. (2023). Nano $CaCO_3$ for enhancing properties of cement-based materials: A comprehensive review. *Journal of Sustainable Cement-Based Materials*, *12*(12), pp. 1475-1494. https://doi.org/10.1080/21650373.2023.2233512

Shen, Z., Baker, W., Ye, H. and Li, Y. (2019). pH-Dependent aggregation and pH-independent cell membrane adhesion of monolayer-protected mixed charged gold nanoparticles. *Royal Society of Chemistry Nanoscale*, 11, pp. 7371-7385. https://doi.org/10.1039/C8NR09617A

Teawpanich, P., Saisinchai, S., Numprasanthai, A., Bissen, R., Juntarasakul, O., Tabelin, C. B. and Phengsaart, T. (2023). Quality Improvement of Low-Grade Calcium Carbonate Using Induced Roll Magnetic Separator. *Engineering Journal*, *27*(10), pp. 1-10. DOI:10.4186/ej.2023.27.10.1

Wang, X., Li, B., Tan, S., Tang, G., Xiang, Z. and Liu, Y. (2024). Characteristics of antimony mineralization in the Yangla polymetallic deposit, northwestern Yunnan, SW China: Insights from calcite Sm-Nd dating and C-O-Sr isotopes, *Ore Geology Reviews*, 173, 106266, https://doi.org/10.1016/j.oregeorev.2024.106266.

Whitworth, A. J., Forbes, E., Verster, I., Jokovic, V., Awatey, B. and Parbhakar-Fox, A. (2022). Review on advances in mineral processing technologies suitable for critical metal recovery from mining and processing wastes. *Cleaner Engineering and Technology*, 7, 100451. https://doi.org/10.1016/j.clet.2022.100451.

Wonyen, D. G., Kromah, V., Gibson, B., Nah, S. and Chelgani, S. C. (2018). A Review of Flotation Separation of Mg Carbonates (Dolomite and Magnesite). *Minerals*, *8*(8), 354. https://doi.org/10.3390/min8080354

Xu, J., Liu, X., Lai, J., He, H., Song, X., Zhai, D., Li, B., Wang, Y., Shi, J. and Zhou, X. (2022). In Situ U-Pb Geochronology of Calcite from the World's Largest Antimony Deposit at Xikuangshan, Southern China. *Minerals*, *12*(7), 899. https://doi.org/10.3390/min12070899.

Yang R., Guo, X., Song, K., Bai, X., Jia, L., Chen, X., Wang, X. and Wang, J. (2021). Influence of pH on the crystal structure of NiMoO4 nanomaterials and their supercapacitor performances, *Ceramics International*, *47*(8). pp. 11349-11357. https://doi.org/10.1016/j.ceramint.2020.12.261